

Article

Dynamic Metasomatism Experiments Investigating the Interaction between Migrating Potassic Melt and Garnet Peridotite

Stephen F. Foley *  and Maik Pertermann

Department of Earth and Environmental Sciences, Macquarie University, North Ryde, NSW 2109, Australia

* Correspondence: stephen.foley@mq.edu.au

Abstract: Dynamic metasomatism experiments were performed by reacting a lamproite melt with garnet peridotite by drawing melt through the peridotite into a vitreous carbon melt trap, ensuring the flow of melt through the peridotite and facilitating analysis of the melt. Pressure (2–3 GPa) and temperature (1050–1125 °C) conditions were chosen where the lamproite was molten but the peridotite was not. Phlogopite was formed and garnet and orthopyroxene reacted out, resulting in phlogopite wehrlite (2 GPa) and phlogopite harzburgite (3 GPa). Phlogopites in the peridotite have higher Mg/(Mg + Fe) and Cr₂O₃ and lower TiO₂ than in the lamproite due to buffering by peridotite minerals, with Cr₂O₃ from the elimination of garnet. Compositional trends in phlogopites in the peridotite are similar to those in natural garnet peridotite xenoliths in kimberlites. Changes in melt composition resulting from the reaction show decreased TiO₂ and increased Cr₂O₃ and Mg/(Mg + Fe). The loss of phlogopite components during migration through the peridotite results in low K₂O/Na₂O and K/Al in melts, indicating that chemical characteristics of lamproites are lost through reaction with peridotite so that emerging melts would be less extreme in composition. This indicates that lamproites are unlikely to be derived from a source rich in peridotite, and more likely originate in a source dominated by phlogopite-rich hydrous pyroxenites. Phlogopites from an experiment in which lamproite and peridotite were intimately mixed before the experiment did not produce the same phlogopite compositions, showing that care must be taken in the design of reaction experiments.

Keywords: reaction experiments; mantle metasomatism; peridotite; lamproite; phlogopite



Citation: Foley, S.F.; Pertermann, M. Dynamic Metasomatism Experiments Investigating the Interaction between Migrating Potassic Melt and Garnet Peridotite. *Geosciences* **2021**, *11*, 432. <https://doi.org/10.3390/geosciences11100432>

Academic Editors: Ian Coulson and Jesus Martinez-Frias

Received: 21 September 2021

Accepted: 15 October 2021

Published: 18 October 2021

Publisher's Note: MDPI stays neutral with regard to jurisdictional claims in published maps and institutional affiliations.



Copyright: © 2021 by the authors. Licensee MDPI, Basel, Switzerland. This article is an open access article distributed under the terms and conditions of the Creative Commons Attribution (CC BY) license (<https://creativecommons.org/licenses/by/4.0/>).

1. Introduction

The xenolith record from the cratonic mantle lithosphere shows that much of the lower lithosphere was originally strongly depleted in melt components and subsequently re-enriched, a process that was titled stealth metasomatism [1]. This re-enrichment may re-introduce clinopyroxene and garnet into harzburgites [2,3] or may lead to the crystallization of hydrous minerals including mica and amphiboles [4,5]. These are Mg-rich where they occur in peridotites because they are buffered by the Mg# (100Mg/(Mg + Fe)) of the modally dominant olivine and pyroxenes, but may have more Fe-rich compositions where they are deposited as discrete rock types in channels from fractionating, flowing melts.

Although the products of reactions between metasomatic agents and peridotites are well documented from a plethora of xenoliths, the nature of the metasomatic agent remains contentious because most reactions have gone to completion, or the melts or fluids have moved on. Initial debates about whether fluids or melts were involved in these reactions have settled in favour of melts [6,7], but the composition of the melts is not well understood. In many cases, the reaction produces enrichment in Fe and Ti and is generally attributed to melts related to earlier incarnations of the host kimberlite [8,9], which leads to rocks of the PIC (phlogopite-ilmenite-clinopyroxene) group. In contrast, the abundance of phlogopite in MARID-type (mica-amphibole-rutile-ilmenite-diopside) enrichments leads

to the conclusion that the melts were rich in potassium, with most favouring a lamproitic or orangeitic composition [10,11].

The origin of orangeites (formerly Group II kimberlites; [12]) is the subject of renewed debate as these are more potassic than kimberlites, occur in the same craton as most MARID xenoliths, and are suggested by some to be the carbonate-rich equivalent of lamproites [13]. Interactions of more than one type of potassic melt with peridotite may thus be relevant to the formation of hydrous minerals during re-enrichment.

We refer to the process of re-enrichment by reaction with passing melts as dynamic metasomatism, deliberately choosing the qualifier “dynamic” to emphasize that reactions are not static, but involve the flow of melt through the peridotite, with reaction products incorporating chemical components from both the melt and the host rock. In the case of crystallization in channels, dynamic metasomatism also occurs at the initial margins of veins and dykes, as seen, for example, in Ligurian peridotites [14], whereas later crystallization in the centre of veins may simply correspond to igneous fractionation from a moving melt. The process of dynamic metasomatism has almost universally been studied in natural rocks but has received little attention in high-pressure experiments. Odling [15,16] tested reactions between depleted peridotites and fluids and kimberlitic melts, finding mica and amphibole to be products of reaction with kimberlitic melt [16], whereas abundant alkali amphibole and less phlogopite were produced from reactions with a water-rich COH fluid [15]. These experiments used long capsules and a temperature gradient to drive melt migration. Here, we investigate reactions between peridotite and a lamproitic melt—another commonly invoked metasomatic agent—using a melt trap to draw the melt through the peridotite.

The purpose of this investigation is twofold: (i) to characterize the mineralogical products of the reaction between peridotite and a passing potassic melt, and (ii) to assess the modification of the composition of the migrating melt. Here, we use a leucite lamproite as the migrating melt, which may be more common at shallower levels of the continental lithosphere, and may represent the more evolved products of fractionation of olivine lamproites [17].

2. Materials and Methods

2.1. Experimental Design

To ensure reaction between peridotite and a migrating melt, the experiments were designed to contain an alkaline melt (lamproite) at one end of the capsule, peridotite in the middle, and a vitreous carbon melt trap at the other end of the capsule (Figure 1). The primary function of the melt trap is to facilitate movement of melt through the peridotite, which works due to the pore space within the trap *initially* offering a lower pressure than in the rest of the capsule. Experiments were conducted with the melt trap at the top of the capsule so that melt movement had to occur against gravity. The ratio of vitreous carbon trap to silicate charge was kept low (0.035–0.046) to allow complete filling of the pore space with melt and subsequent equilibration of the melt: this allows equilibration of the melt within 24 h [18], circumventing issues with the attainment of equilibrium [19–21], which only occurs when the pore space in the trap is too large [18]. All experiments in this study were run for 24 h or more. A similar constellation of three layers was used for basalt/peridotite experiments, but with a larger melt trap that was not intended to collect melts for analysis [22,23].

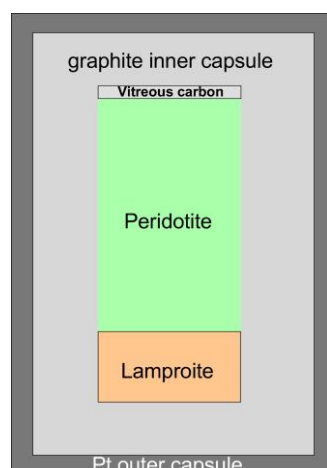


Figure 1. Capsule design for dynamic metasomatism experiments. Lamproite loaded below peridotite as separate layers so that melt must flow against gravity, drawn through by suction of the vitreous carbon melt trap, present at 3.5–4.5% of the volume of the silicate charge. Inner graphite capsule prevents iron loss to outer sealed Pt capsule.

Graphite-lined Pt capsules were used to limit the loss of iron during the experiments: the Pt capsules had an inner diameter of 3.6 mm and the graphite liners had an inner diameter of 1.9–2.0 mm. Water was added to the charge, then the capsule was welded shut whilst cooled below 0 °C in an iced brass block. After welding, capsules were checked for leaks by heating at 110 °C for >30 min and re-weighing. The amount of water was ≈10 wt% for the lamproite and ≈3 wt% for the whole charge; this amount of water ensures that the lamproite is molten under the P-T conditions of the experiments [24]. One experiment (G141, 3 GPa, 1100 °C) was run with the peridotite and lamproite intimately mixed before the experiment to compare results with those of the layered configuration. This should produce similar mineral assemblages to the reaction zone, but in which minerals are easier to identify [25,26].

Experiments were conducted at 2 and 3 GPa in standard piston-cylinder apparatuses at the University of Göttingen as part of the Diploma thesis of M. Pertermann [27]. Boron nitride was used for sample sleeves and NaCl as pressure medium apart from the 1250 °C experiment at 3 GPa, for which BaCO₃ was used as the melting point of NaCl was exceeded. Temperature was controlled to within ±1 °C by an 818P Eurotherm controller and Pt/Pt₉₀Rh₁₀ thermocouples and run durations varied between 24 and 132 h. After experiments, capsules were cut lengthwise with a WS22 wire saw and the resulting halves and thin sample discs were mounted in epoxy and polished with diamond paste. Details of experiments are listed in Table 1.

Table 1. Experimental details for dynamic metasomatism experiments.

Experiment Label	Pressure GPa	Temperature °C	Duration Hours	Ratio Peridotite/Lamproite ^a	Ratio Trap/Silicate Charge ^b	Phases Present ^c
G132	2	1050	72	3.29	0.043	OL + CPX + PHL + L
G128	2	1125	72	2.52	0.039	OL + CPX + PHL + L
G138	3	1100	24	3.15	0.046	OL + CPX + OPX + PHL + L
G131	3	1100	58	2.57	0.043	OL + CPX + OPX + PHL + L
G137	3	1100	132	3.18	0.044	OL + CPX + OPX + PHL + L
G139	3	1250	24	3.19	0.041	OL + (SP) + L
G141 *	3	1100	72	3.19	0.036	OL + (CPX) + OPX + PHL + L

^a = weight ratio peridotite/lamproite in capsule; ^b = weight ratio of carbon extraction trap to total silicate mix; ^c = phases present in peridotite section after experiment; * = peridotite and lamproite intimately mixed before experiment.

2.2. Starting Materials and Analytical Methods

The alkaline melt is a natural lamproite from Gaussberg, eastern Antarctica, chosen because of its suitable composition and because phase relations at these pressures are known from previous studies [24,28]. The peridotite is a natural garnet lherzolite from Jagersfontein, South Africa, which has also been used previously in experiments, commonly as mineral separates. Compositions of the rocks and the constituent minerals of the peridotite are given in Table 2.

Table 2. Compositions of starting materials: lamproite and peridotite and its constituent minerals.

Starting Material	65%		15%		10%		Average
	Gaussberg	J4	J4	J4	J4	J4	Garnet
	Lamproite	Peridotite	Olivine	Opx	Cpx	Grt	Lherzolite
SiO ₂	51.1	44.88	40.8	57.58	55.14	42.1	45.98
TiO ₂	3.3	0.18	0.03	0.23	0.49	0.78	0.09
Al ₂ O ₃	10.28	2.56	0.04	0.98	2.89	20.93	1.57
MgO	7.08	40.89	48.98	33.94	18.11	21.51	43.46
FeO	6.08	8.56	9.94	6.08	4.05	7.81	6.91
CaO	4.03	2.19	0.07	1.02	15.65	4.25	1.16
Na ₂ O	1.8	0.3	0.03	0.32	2.25	0.11	0.16
K ₂ O	12.46	0.01	0.01	0.01	0.03	0.01	0.12
Cr ₂ O ₃	0.03	0.34	0.03	0.21	0.82	2.02	0.32
MnO	0.08	0.13	0.11	0.12	0.13	0.28	0.11
NiO	0.01	0.23	0.36				0.29
BaO	0.55						
P ₂ O ₅	1.37						
H ₂ O	1.17						
Sum	99.34	100.27	100.4	100.49	99.56	99.8	100.17
Mg#	67.49	89.49	89.78	90.87	88.85	83.08	91.81

The melt trap consisted of 60–80 µm grains of vitreous carbon (Deutsche Carbone AG, Frankfurt) and was used in preference to diamond aggregates for the melt trap since it simplifies polishing of experimental charges and quenched melts. Trace element analysis shows that the only major contaminant in the vitreous carbon is Zr (1340 ppm) with minimal amounts of Ba (18 ppm) and Rb (4.7 ppm).

The lamproite is a glassy pillow rim sample (4891-3) of the Gaussberg lamproite with a composition close to the range given by Sheraton and Cundari ([29] Table 2). The sample was crushed and ground under acetone in an agate mortar; the resulting grain size was mostly 20–30 µm with a maximum of 50 µm. Previous experiments [24] show that at 2 GPa and 1125 °C the lamproite should be completely molten, whilst at 2 GPa and 1050 °C and at 3 GPa and 1100 °C phlogopite coexists with a large amount of melt, ensuring adequate reaction with the peridotite.

The modal mineral composition of the J4 garnet lherzolite was estimated by XRD analysis to be 65% olivine, 15% orthopyroxene, 10% clinopyroxene and 15% garnet. The resulting calculated bulk composition of the rock and the mineral analyses are given in Table 2.

Electron microprobe analyses of run products were obtained at Heidelberg (Cameca SX-51, Cameca, Paris, France), Utrecht (JEOL JXA 8600 Superprobe, JEOL, Tokyo, Japan) and Macquarie (Cameca SX100, Cameca, Paris, France) Universities using standard analytical procedures (15 kV, 10–20 nA) calibrated on a variety of natural and synthetic mineral standards. For phlogopites and quenched melts, the beam was defocused to 10–15 µm whereas for all other minerals a focused beam (1–2 µm) was used.

3. Results

3.1. Phases Present in Experimental Products

Experiments were conducted at 2 and 3 GPa, two temperatures at each pressure and a time series of three experiments was conducted at 3 GPa and 1100 °C with durations of 24, 58 and 132 h. A summary of experimental run conditions, ratios of starting materials and experimental products is given in Table 1. Experiment G141 with the peridotite and lamproite intimately mixed produced olivine, Cpx, Phl and melt, the same assemblage as in the experiments with layered run charges, but mineral compositions differed (see below).

Inspection of the polished sections showed that the layering of the run charges remained essentially intact and the dimensions of the original lamproite and peridotite remained constant. Abundant quench phlogopite formed in the lamproite sections, where phlogopite also occurred as idiomorphic primary platelets up to $50 \times 50 \mu\text{m}$. No melts or continuous pathways could be identified in the peridotite section, but phlogopite occurred as interstitial patches up to $100 \mu\text{m}$ in length and $50 \mu\text{m}$ wide. Minerals adjacent to the phlogopites in the peridotite section were rounded and/or embayed, indicating reaction with a melt and deposition of the phlogopite in the interstices (Figure 2). All minerals in the peridotite showed thin rims with modified compositions due to reaction with passing melt: these rims were too thin for microprobe analysis (Figure 2).

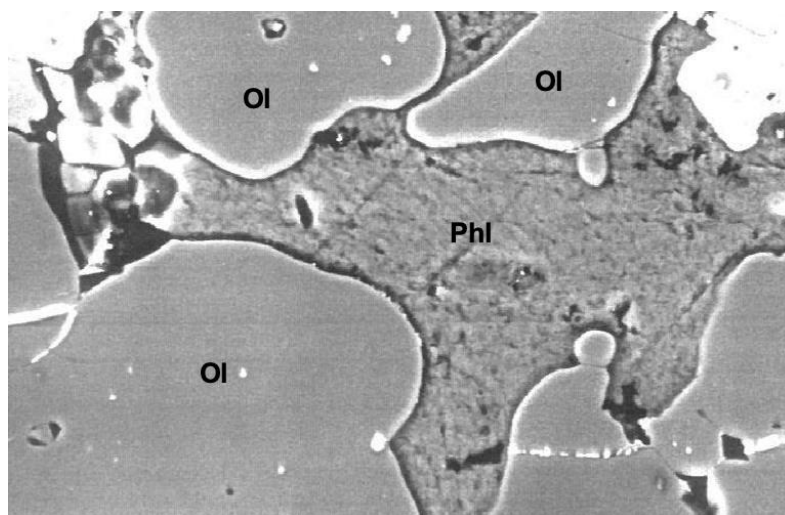


Figure 2. Back-scattered electron image of the peridotite section after Experiment G128 at 2 GPa and 1125 °C (Ol + Cpx + Phl). Compositionally homogeneous xenomorphic phlogopite crystallizes interstitially between olivine and clinopyroxene. Olivine shows rounded and embayed grains indicating reaction (Melt + olivine \Rightarrow Phl) and light, Fe-rich rims due to approaching equilibrium of Mg# with the infiltrating melt.

In both experiments at 2 GPa, run products contained olivine, Cpx, Phl and melt, but no Opx or garnet could be found, whereas at 3 GPa and 1100 °C olivine, Opx, minor Cpx, Phl and melt formed. The time-series experiments showed the same run products regardless of duration.

3.2. Mineral Compositions

3.2.1. Phlogopite

Phlogopites were analysed in the remains of the lamproite section, in the peridotite close to the lamproite section and in the peridotite close to the melt trap in order to establish any systematic compositional variation across the profile of the peridotite section. Two compositional groups could be identified; one in the lamproite section with high TiO_2 and low Cr_2O_3 (Table 3), and the other in the peridotite section with lower TiO_2 and higher Cr_2O_3 . No systematic variation could be recognized for phlogopites in the peridotite

section (Figure 3) and so these are summarized in unison in Table 3. Phlogopites in the time series comparison (G138, 24 h; G131, 58 h; G137, 132 h) showed only small compositional differences with no consistent trend: phlogopite from the shortest and longest time-series runs were most similar, whereas those in the experiment with intermediate duration had a higher Al_2O_3 and lower Cr_2O_3 , which may be attributable to the higher proportion of lamproite in the capsule imparting stronger lamproite characteristics.

Table 3. Phlogopite compositions in dynamic metasomatism experiments.

Expt	G132		G132		G128		G128	
P (GPa)	2		2		2		2	
T (°C)	1050		1050		1125		1125	
Duration (h)	72		72		72		72	
Location	Residual melt	s.d.	interstitial in peridotite	s.d.	Residual melt	s.d.	interstitial in peridotite	s.d.
SiO ₂	40.29	0.12	39.7	0.27	39.73	0.24	38.72	0.51
TiO ₂	5.14	0.43	1.2	0.08	6.98	0.37	1.26	0.11
Al ₂ O ₃	11.86	0.1	14.7	0.28	11.49	0.27	15.99	0.43
MgO	20.12	0.36	23.2	0.17	17.98	0.22	22.4	0.25
FeO	6.19	0.22	3.7	0.14	7.42	0.2	3.68	0.09
CaO	0.03	0.05	0.0	0.02	0.05	0.03	0.03	0.02
Na ₂ O	0.12	0.02	0.6	0.03	0.16	0.03	0.74	0.04
K ₂ O	9.98	0.11	9.4	0.16	9.81	0.16	9.32	0.09
Cr ₂ O ₃	0.17	0.07	1.7	0.21	0.07	0.02	1.67	0.2
MnO	0.05	0.03	0.0	0.02	0.05	0.03	0.05	0.03
NiO	0.08	0.03	0.2	0.04	0.04	0.02	0.14	0.07
BaO	0.29	0.04	0.2	0.06	0.35	0.03	0.22	0.06
Sum	94.32		94.58		94.13		94.22	
Mg#	85.3		91.8		81.2		91.6	
n	5		14		5		8	
Expt	G138		G138		G131		G131	
P (GPa)	3		3		3		3	
T (°C)	1100		1100		1100		1100	
Duration (h)	24		24		58		58	
Location	Residual melt	s.d.	interstitial in peridotite	s.d.	Residual melt	s.d.	interstitial in peridotite	s.d.
SiO ₂	40.97	0.84	39.31	0.53	40.97	0.38	39.22	0.19
TiO ₂	2.56	0.62	1.12	0.24	4.67	0.43	1.19	0.22
Al ₂ O ₃	13.97	0.58	15.27	0.34	11.84	0.15	14.3	0.26
MgO	23.15	0.47	23.52	0.57	20.08	0.33	22.53	0.3
FeO	5.09	0.2	4.47	0.22	5.7	0.21	4.28	0.56
CaO	0.04	0.02	0.03	0.03	0.19	0.25	0.02	0.02
Na ₂ O	0.28	0.07	0.42	0.07	0.11	0.02	0.28	0.11
K ₂ O	8.78	0.23	8.54	0.26	10.06	0.22	9.88	0.09
Cr ₂ O ₃	0.56	0.38	1.39	0.26	0.18	0.03	1.25	0.23
MnO					0.03	0.01	0.03	0.02
NiO	0.1	0.06	0.18	0.04	0.04	0.03	0.13	0.07
BaO	0.36	0.09	0.4	0.08	0.31	0.06	0.39	0.09
Sum	95.86		94.65		94.18		93.5	
Mg#	89.0		90.4		86.3		90.4	
n	8		11		5		12	
Expt	G137		G137					
P (GPa)	3		3					
T (°C)	1100		1100					
Duration (h)	132		132					
Location	Residual melt	s.d.	interstitial in peridotite	s.d.				
SiO ₂	39.36	1.09	39.85	0.93				
TiO ₂	3.1	0.49	1.07	0.56				
Al ₂ O ₃	13.76	0.43	15.1	0.53				
MgO	23.03	0.34	23.89	0.42				
FeO	4.41	0.21	4.21	0.14				
CaO	0.02	0.01	0.02	0.02				
Na ₂ O	0.14	0.02	0.24	0.04				
K ₂ O	9.09	0.22	8.91	0.2				
Cr ₂ O ₃	0.68	0.13	1.41	0.42				
MnO								
NiO	0.08	0.03	0.16	0.03				
BaO	0.28	0.08	0.3	0.06				
Sum	93.95		95.16					
Mg#	90.3		91.0					
n	6		16					

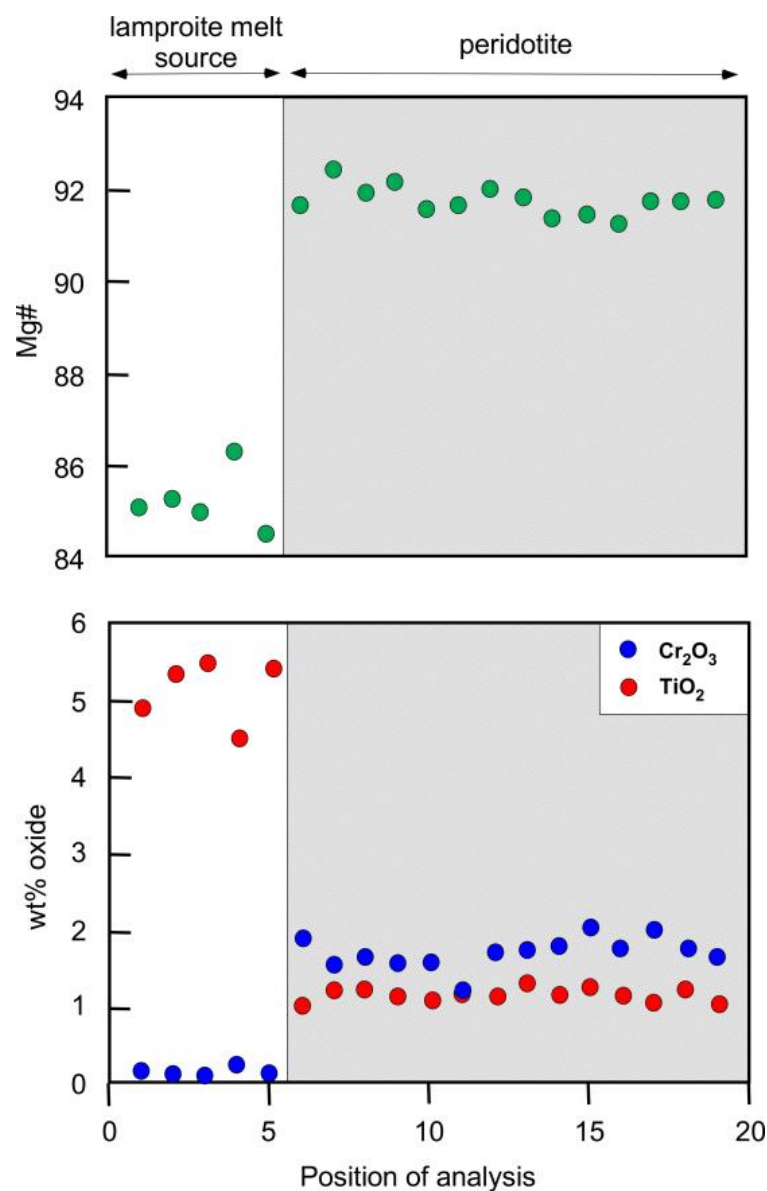


Figure 3. Traverse of phlogopite compositions in lamproite and peridotite sections of Experiment G132 (2 GPa, 1050 °C), plotted at approximately equal intervals from bottom to top of capsule (left to right). Peridotite section indicated by grey background. New phlogopites grown in the peridotite have higher Mg# and Cr₂O₃ as well as lower TiO₂ than those crystallizing as a liquidus phase in the lamproite and show consistent compositions throughout the peridotite section.

In the 2 GPa experiments, phlogopites in the higher temperature experiment (1125 °C vs. 1050 °C) have slightly higher TiO₂ (7.0 vs. 5.1 wt%) and lower Cr₂O₃ (0.07 vs. 0.17 wt%), emphasizing the polarization between mineral compositions in the lamproite and peridotite sections. Phlogopite did not occur at 2 GPa and 1125 °C in the liquidus experiments of [24], presumably due to a higher content of fluid components in those experiments. Phlogopites in the peridotite sections are distinct from those in the lamproite section, with higher Cr₂O₃ (\approx 1.7 vs. \leq 0.2 wt%), Al₂O₃ (15–16 vs. <12 wt%) and Na₂O (0.60–0.74 vs. 0.12–0.16 wt%) and lower TiO₂ (1.0–1.3 vs. >5 wt%; Figure 3). The Mg# is buffered by the peridotite minerals at 90.4–91.8, in contrast to those in the lamproite section, which are more variable (Figure 3) and characteristic of those in magmatic lamproites [17]. The distinction between phlogopites in the peridotite reaction zone and the lamproite section for experiment G131 at 3 GPa, 1100 °C (Figure 4) is not as sharp as in Figure 3. This is most likely due to the higher proportion of

lamproite relative to peridotite (i.e., melt/rock ratio is higher) in the experiment (Table 1), as the higher temperature did not have this effect in other experiments.

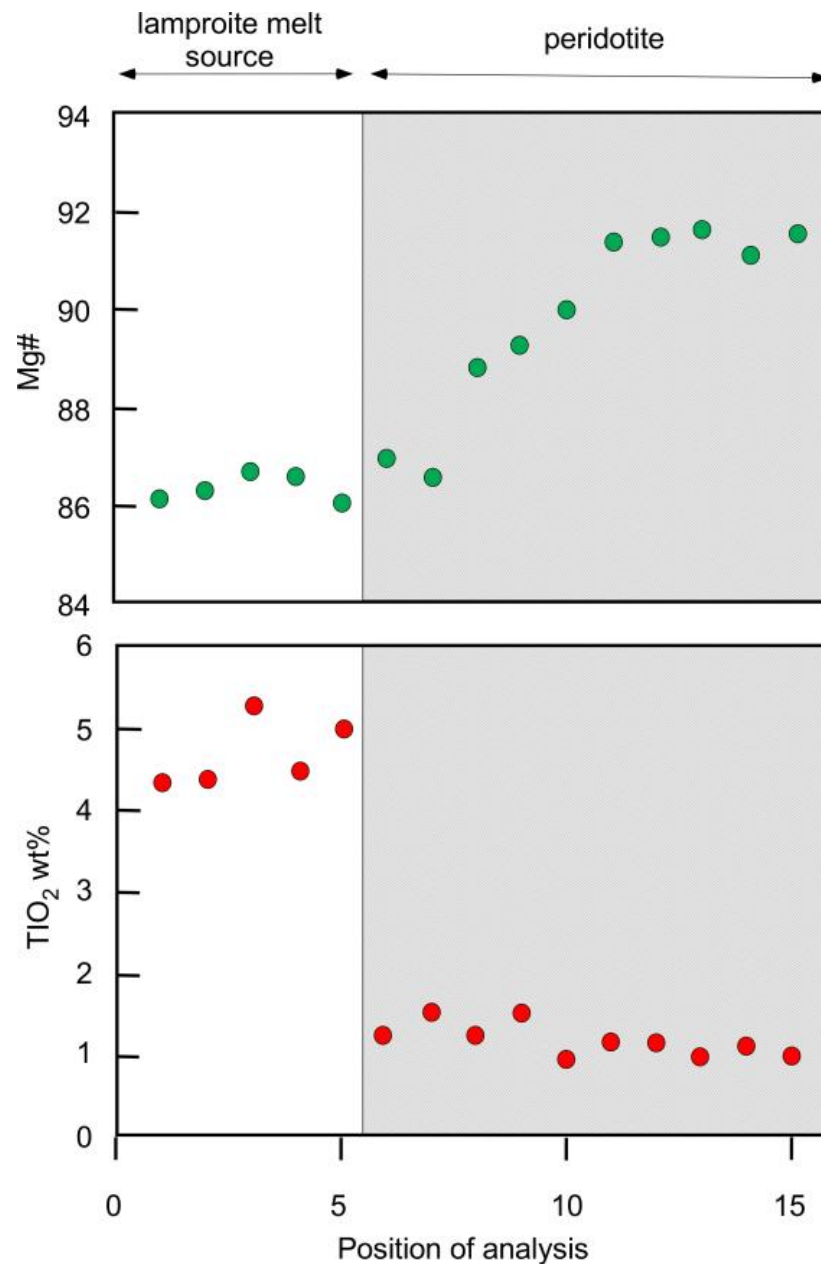


Figure 4. Traverse of phlogopite compositions in lamproite and peridotite sections of Experiment G131 (3 GPa, 1100 °C), plotted from bottom to top of capsule (left to right). Trends are similar to those in Figure 3 but the lamproite characteristics are beginning to dominate the Mg# at the start of the peridotite section, probably due to the higher proportion of lamproite in this experiment.

3.2.2. Other Silicate Minerals

All silicate minerals display compositional changes compared to the mineral composition of the starting materials: the values listed in Table 4 are averages of points analysed as line scans as for the phlogopites in Figure 3, with the low standard deviations indicating relatively uniform compositions. Clinopyroxenes are diopsides with Mg# 88–91, Cr₂O₃ between 0.85 and 1.37 wt%, Al₂O₃ between 2.6 and 3.5 wt%, and Na₂O 0.6 to 1.6 wt%. Orthopyroxenes have Mg# 88.6–90.2, Cr₂O₃ between 0.24 and 0.59 wt%, Al₂O₃ between 1.2 and 2.0 wt%, and Na₂O 0.17–0.19 wt%.

Table 4. Compositions of peridotite minerals in dynamic metasomatism experiments.

Expt	G132		G128		G138		G131		G137	
P (GPa)	2		2		3		3		3	
T (°C)	1050		1125		1100		1100		1100	
Duration (h)	72		72		24		58		132	
Mineral	CPX	s.d.	CPX	s.d.	CPX	s.d.	CPX	s.d.	CPX	s.d.
SiO ₂	53.06	0.53	53.9	1.11	54.32	0.48	53.86	0.26	53.93	0.65
TiO ₂	0.28	0.03	0.5	0.12	0.15	0.05	0.17	0.03	0.33	0.18
Al ₂ O ₃	3.15	0.52	3.5	0.7	2.61	0.18	3.06	0.23	2.67	0.45
MgO	17.74	0.28	18.0	0.56	18.83	0.31	18.38	0.4	17.72	1.01
FeO	3.08	0.16	3.8	0.39	3.44	0.37	3.37	0.09	4.18	1.09
CaO	20.48	0.27	17.3	1.7	18.57	0.3	18.33	0.35	19.05	0.45
Na ₂ O	0.62	0.04	1.6	0.64	0.98	0.12	1.11	0.14	1.28	0.27
K ₂ O	0.01	0.01	0.0	0.02	0.02	0.01	0.01	0.01	0.03	0.01
Cr ₂ O ₃	1.29	0.15	1.0	0.16	1.33	0.46	1.37	0.15	0.85	0.65
MnO	0.12	0.02	0.1	0.03			0.12	0.03		
NiO	0.04	0.02	0.1	0.01	0.05	0.03	0.04	0.02	0.04	0.05
Sum	99.87		99.72		100.3		99.82		100.08	
Mg#	91.1		89.4		90.7		90.7		88.3	
n	9		28		18		12		16	
Expt	G132		G128		G138		G131		G137	
P (GPa)	2		2		3		3		3	
T (°C)	1050		1125		1100		1100		1100	
Duration (h)	72		72		24		58		132	
Mineral	OL	s.d.	OL	s.d.	OL	s.d.	OL	s.d.	OL	s.d.
SiO ₂	40.45	0.17	40.32	0.19	41.61	0.58	40.64	0.12	41.38	0.23
TiO ₂	0.02	0.01	0.03	0.02	0.03	0.02	0.01	0.01	0.03	0.02
Al ₂ O ₃	0.02	0.01	0.03	0.01	0.06	0.06	0.04	0.01	0.02	0.02
MgO	48.85	0.22	48.84	0.19	48.74	0.36	48.8	0.22	49.02	0.28
FeO	10.38	0.27	10.31	0.2	10.77	0.45	10.43	0.29	11.31	0.37
CaO	0.09	0.01	0.11	0.03	0.11	0.02	0.08	0.01	0.08	0.02
Na ₂ O	0.01	0.01	0.01	0.01	0.02	0.02	0.01	0.01	0.02	0.02
K ₂ O	0	0	0	0	0.03	0.05	0	0.01	0	0
Cr ₂ O ₃	0.04	0.01	0.06	0.01	0.09	0.08	0.06	0.01	0.07	0.04
MnO	0.16	0.04	0.14	0.03			0.15	0.02		
NiO	0.35	0.05	0.36	0.04	0.26	0.04	0.38	0.03	0.29	0.05
Sum	100.37		100.21		101.72		100.6		102.22	
Mg#	89.3		89.4		89.0		89.3		88.5	
n	12		19		14		9		6	
Expt	G139		G138		G131		G137			
P (GPa)	3		3		3		3			
T (°C)	1250		1100		1100		1100			
Duration (h)	24		24		58		132			
Mineral	OL	s.d.	OPX	s.d.	OPX	s.d.	OPX	s.d.		
SiO ₂	40.63	0.35	57.58	0.52	56.4	0.58	57.14	0.93		
TiO ₂	0.02	0.02	0.19	0.06	0.13	0.03	0.18	0.06		
Al ₂ O ₃	0.03	0.01	1.41	0.57	2.01	0.53	1.22	0.37		
MgO	50.43	0.56	32.93	95	33.13	0.39	33.48	0.75		
FeO	8.81	0.41	7.54	1.24	6.39	0.42	7.35	0.87		
CaO	0.12	0.02	1.36	0.23	1.21	0.06	1.13	0.08		
Na ₂ O	0.01	0.01	0.19	0.08	0.17	0.05	0.17	0.07		
K ₂ O	0.01	0.02	0.01	0.04	0.01	0.01	1	0.07		
Cr ₂ O ₃	0.21	0.07	0.3	0.36	0.59	0.28	0.24	0.16		
MnO					0.15	0.03				
NiO	0.17	0.09	0.06	0.03	0.12	0.02	0.07	0.04		
Sum	100.44		101.57		100.31		101.984			
Mg#	91.1		88.6		90.2		89.0			
n	21		12		10		23			

In the shortest run of the time series, Opx has higher Al₂O₃ and Cr₂O₃ contents (1.6 vs. 1.3 wt% and 0.5 vs. 0.2 wt%) and lower FeO contents (7.2 vs. 7.7 wt%) near the carbon trap, which may reflect less reaction with the percolating melt. Olivine displays uniform composition throughout the peridotite layer, with Mg# ranging from 88.5 to 91.1.

3.3. Melt Compositions

The quenched melts were analysed in the residual lamproite melt and in the melt traps (Table 5); only in one high-temperature experiment was interstitial melt found in the peridotite section. However, the analysis of the melts in the residual lamproite was

complicated by the occurrence of abundant quench crystals, mainly phlogopite. The discrepancy in the total from 100% is principally due to H₂O, but minor CO₂ may have been generated from the graphite capsule; the concentration of water was not determined independently.

Table 5. Melt compositions in dynamic metasomatism experiments.

Expt	G132		G132		G128		G128	
P (GPa)	2		2		2		2	
T (°C)	1050		1050		1125		1125	
Duration (h)	72		72		72		72	
	Residual melt	s.d.	Melt trap	s.d.	Residual melt	s.d.	Melt trap	s.d.
SiO ₂	56.33	2.14	52.49	2.92	55.54	0.30	48.63	2.42
TiO ₂	2.98	0.26	1.24	0.25	2.41	0.13	1.32	0.21
Al ₂ O ₃	10.10	0.15	14.96	1.20	10.62	0.09	15.44	1.04
MgO	3.61	2.40	8.21	2.18	3.14	0.76	8.57	1.44
FeO	5.58	0.64	5.21	1.01	4.79	0.17	5.89	0.59
CaO	4.18	0.39	4.96	2.05	2.09	0.11	8.52	2.99
Na ₂ O	1.57	0.28	2.22	0.46	1.93	0.15	3.00	0.67
K ₂ O	7.59	0.26	5.82	1.04	11.20	0.18	3.93	0.84
Cr ₂ O ₃	0.01	0.02	0.09	0.04	0.01	0.01	0.09	0.04
MnO	0.10	0.03	0.12	0.06	0.09	0.02	0.15	0.07
NiO	0.01	0.02	0.03	0.04	0.01	0.01	0.02	0.03
BaO	0.65	0.06	0.13	0.06	0.66	0.05	0.07	0.04
P ₂ O ₅	2.28	0.30	0.39	0.25	1.66	0.08	0.39	0.09
Sum	94.98		95.87		94.16		96.01	
Mg#	53.5		73.7		53.8		72.2	
n	8		23		7		23	
Expt	G138		G138		G131		G131	
P (GPa)	3		3		3		3	
T (°C)	1100		1100		1100		1100	
Duration (h)	24		24		58		58	
	Residual melt	s.d.	Melt trap	s.d.	Residual melt	s.d.	Melt trap	s.d.
SiO ₂	41.75	1.89	44.58	1.92	52.01	1.53	43.68	2.74
TiO ₂	3.24	0.93	2.08	0.32	3.02	0.21	2.09	0.48
Al ₂ O ₃	12.23	1.44	10.34	1.25	10.21	0.40	10.20	1.88
MgO	16.36	5.61	13.92	2.83	5.45	2.37	13.28	2.96
FeO	6.85	2.25	8.67	1.39	5.39	0.59	8.59	1.41
CaO	5.41	2.91	7.37	1.55	3.73	0.61	7.16	3.12
Na ₂ O	0.75	0.35	2.15	0.60	2.08	0.33	1.74	0.47
K ₂ O	6.67	2.23	4.72	0.97	8.61	0.28	5.71	1.74
Cr ₂ O ₃	0.03	0.04	0.11	0.06	0.02	0.02	0.12	0.14
MnO	0.00	0.00	0.00		0.12	0.01	0.18	0.06
NiO	0.07	0.05	0.02	0.03	0.02	0.02	0.04	0.04
BaO	0.47	0.21	0.32	0.18	0.63	0.07	0.41	0.16
P ₂ O ₅	0.09	0.10	0.60	0.30	2.01	0.33	1.54	0.69
Sum	93.90		94.89		93.30		94.76	
Mg#	81.0		74.1		64.3		73.4	
n	11		11		9		23	
Expt	G137		G139		G139		G139	
P (GPa)	3		3		3		3	
T (°C)	1100		1250		1250		1250	
Duration (h)	132		24		24		24	
	Melt trap	s.d.	Residual melt	s.d.	interstitial in peridotite	s.d.	Melt trap	s.d.
SiO ₂	42.70	1.89	49.06	0.81	51.03	0.40	50.46	2.28
TiO ₂	2.63	0.23	1.87	0.07	1.83	0.10	1.47	0.22
Al ₂ O ₃	10.01	0.84	9.60	0.13	9.80	0.21	10.82	0.89
MgO	14.07	2.27	14.76	2.02	11.96	1.76	13.23	3.71
FeO	9.11	1.19	6.80	0.18	6.83	0.38	5.65	1.09
CaO	5.82	1.85	5.88	1.38	7.51	1.32	6.46	1.17
Na ₂ O	2.64	0.87	0.60	0.08	0.53	0.09	1.25	0.39
K ₂ O	6.10	1.32	4.62	0.43	4.32	0.34	5.27	1.13
Cr ₂ O ₃	0.06	0.06	0.41	0.09	0.38	0.08	0.39	0.13
MnO	0.00	0.00	0.00	0.00	0.00	0.00	0.00	0.00
NiO	0.03	0.04	0.01	0.02	0.01	0.02	0.03	0.05
BaO	0.54	0.17	0.31	0.05	0.33	0.06	0.37	0.10
P ₂ O ₅	0.56	0.70	0.57	0.06	0.54	0.08	0.48	0.15
Sum	94.27		94.50		95.07		95.88	
Mg#	73.4		79.5		75.7		80.7	
n	14		10		12		11	

Melt compositions in the extraction traps were not of uniform composition, but displayed a compositional range, varying with each melt pool analysed, possibly reflecting different extents of melt mixing along paths with different degrees of interaction rather than inhomogeneous

generality of analyses. Glass in the melt trap is quench-free, eliminating the possibility that the variation is due to quenching modification of the melt composition. The individual analyses span a wide range of SiO_2 , and the behaviour of Al_2O_3 and K_2O as a function of the SiO_2 content for experiment G128 (2 GPa, 1125 °C) is shown in Figure 5; this behaviour is representative for all other experiments. The major elements seem to be largely unaffected by the different time scales of the experiments, except for Ti, Na, K and Ba. All these elements are more enriched in the extraction trap of the longer duration experiment, indicating either slower diffusion processes for them, or they reacted more during migration through the peridotite. This is especially the case for Ba, for which the concentration is nearly twice as high in the longer duration experiment than in the shorter experiment.

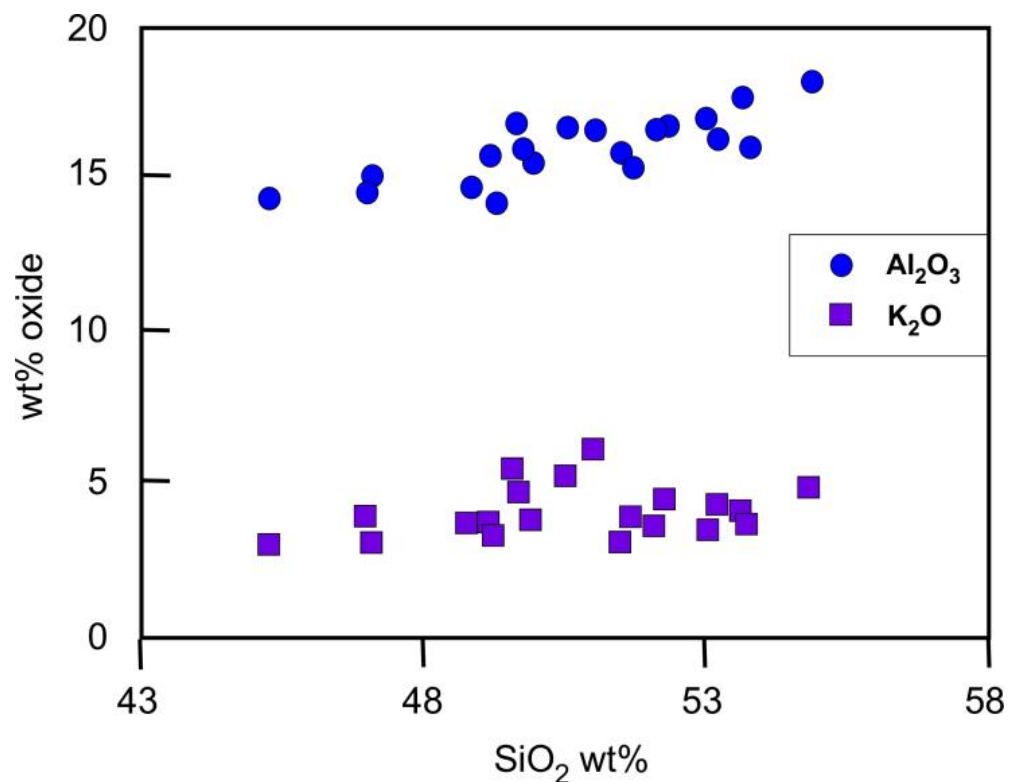


Figure 5. Melt compositions in the melt traps from Experiment G128 (2 GPa, 1125 °C). SiO_2 , Al_2O_3 and K_2O contents show variation, probably due to different path lengths through the peridotite.

In most experiments the melts in the extraction traps have a significantly higher Mg# than the residual lamproite melt (averages 74.6 vs. 66.4), lower $\text{K}_2\text{O}/\text{Na}_2\text{O}$ (averages 2.7 vs. 6.3) and also lower BaO, $\text{K}_2\text{O}/\text{Na}_2\text{O}$ and K/Al ratios (averages 0.50 vs. 0.80). This reflects the uptake of K_2O and Ba in phlogopites that grew in the peridotite and the buffering of the Mg# by the peridotite minerals because the volume of the peridotite greatly exceeds that of the reacting melt. The compositions of melts in the residue of the lamproite section are much less variable than melts in the carbon traps, particularly in terms of Mg# (Figure 6b). Examples of compositional parameters are shown in Figure 6.

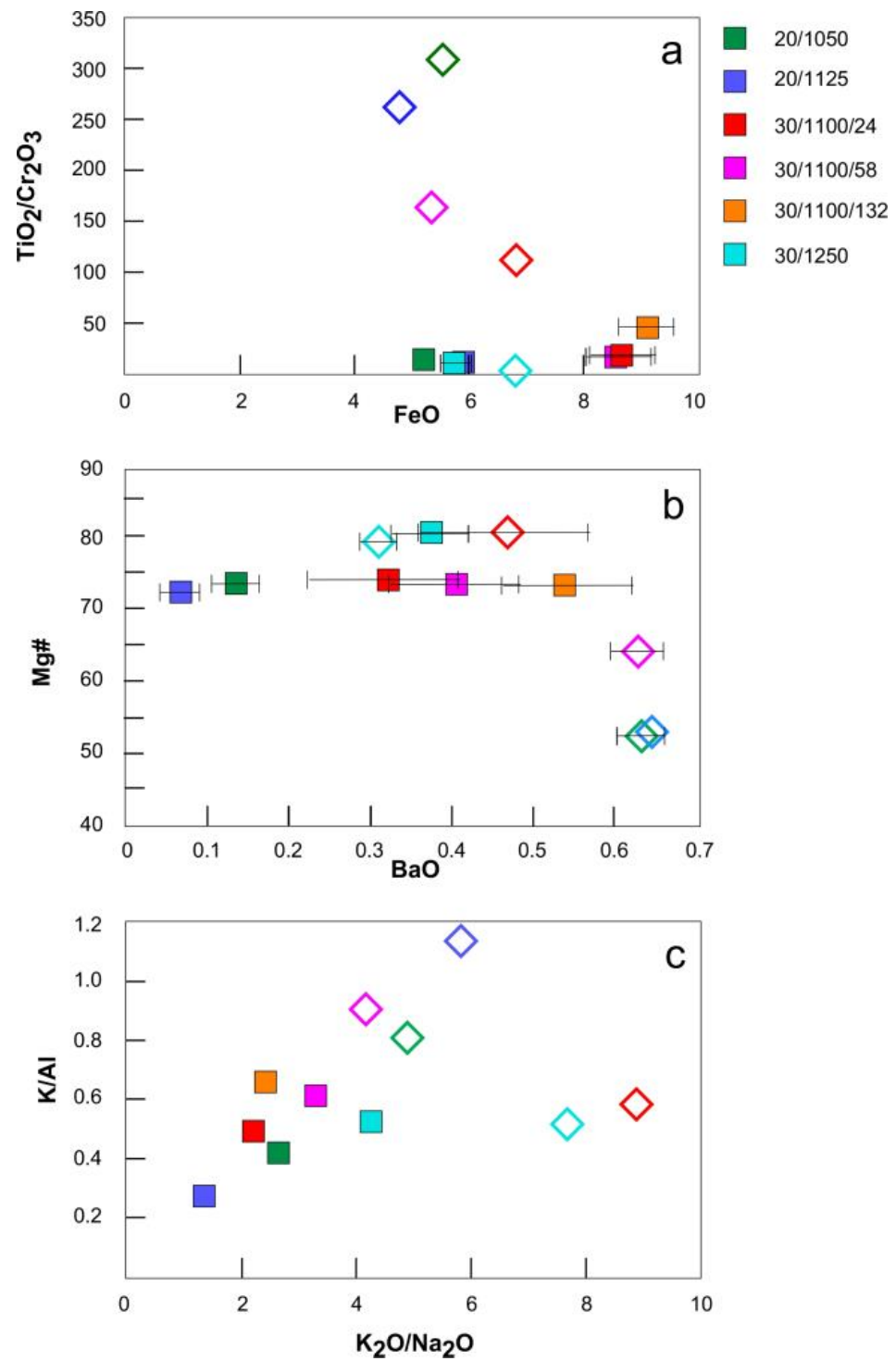


Figure 6. Comparison of melt compositions in melt traps (squares) with melts in the residual lamproite section (diamonds): each symbol is the average for one experiment and colours indicate same experiments (see key). Changes across the peridotite reaction column show similar trends to phlogopites due to buffering of the melt $Mg\#$ by the peridotite (middle) and the uptake of TiO_2 but release of Cr_2O_3 in the metasomatic reaction (a). The growth of phlogopite in the peridotite also results in lower BaO and near-constant $Mg\#$ (b), and in lower K_2O , hence lower K/Al and K_2O/Na_2O (c).

4. Discussion

4.1. Reaction Experiment Design

Reaction experiments have been used increasingly over the last ten years to study hybridization reactions between melts and rocks they pass through, mostly peridotites. One of two methods are usually used: either (i) two rocks (or powdered rocks) are placed in capsules as separate blocks or cylinders with a sharp boundary between them similar to the layered configuration used here (“reaction experiments” using the terminology of Wang and Foley [30]; or (ii) the two powdered rocks are intimately mixed in different proportions (“mixed experiments” in [30]). Layered experiments have been used to assess hybridization by a variety of melts from clastic sedimentary or carbonate-rich through basalt to granite [22,23,31–37]. A similar array of melts has been studied with the mixing of the two reactant rocks [38–41], but few studies have used both methods to compare them. Of these, the experiments of [30] compared mineral compositions using the two methods, concluding that they were the same and that the homogenized mixtures were, therefore, useful to study minerals in thin reaction layers in layered experiments where the formation of new minerals had created a barrier to melt flow.

Experiment G141 was conducted with a homogenized mixture of lamproite and garnet lherzolite in the same ratio as the layered experiment (Table 1) in order to compare results to those from experiments with the layered run charges. This experiment was also run at the same pressure and temperature as the time series experiments. In Figure 7, the compositions of the phlogopites from this experiment are compared to those in layered experiment G131, which had the most similar experiment duration (58 vs. 72 h). Figure 7 shows that the phlogopites from the experiment with the homogenised starting materials are distinct from those in both the peridotite layer and the lamproite residue from Experiment G131: they have low TiO₂ resembling those in the peridotite layer, but high SiO₂ characteristic of those in the lamproite residue. The difference to earlier experimental studies in which similar mineral compositions were found in layered and mixed experiments lies in the inclusion of the carbon melt trap, which has effectively removed the melt components from the reacting system, creating a “flow-through” scenario: the phlogopites in the peridotite layer mimic the reaction products from a flowing melt that is no longer present in the system.

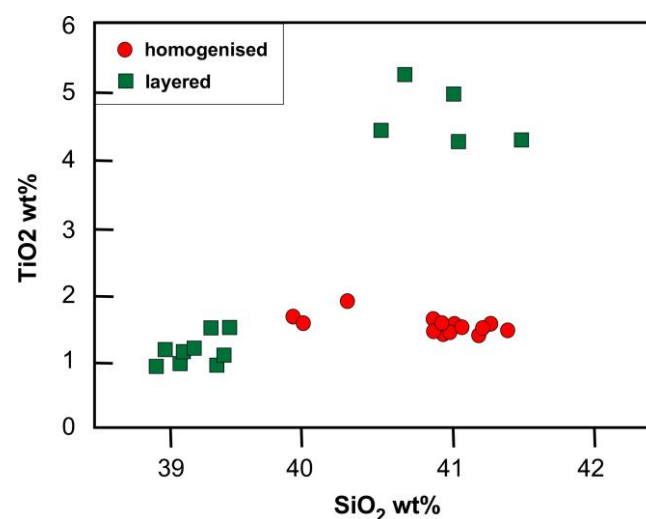


Figure 7. Comparison of phlogopite compositions in layered experiment G131 (green squares) to those in homogenized experiment G141 (both experiments were conducted at 3 GPa, 1100 °C). This shows that minerals from experiments in which lamproite and peridotite are mixed before the experiment (G141) are not equivalent to reaction products in the peridotite section of layered runs.

The use of melt traps has had a chequered history since its introduction to separate fluids and melts from rock matrices to optimize chemical analysis [20,42,43]. Tests have shown that the melt compositions in traps may correspond to melts in equilibrium at

lower pressures than the nominal experimental pressure due to the initial pore space in the traps [19], but that this can be circumvented by ensuring that the volume of the pore space in the trap is exceeded by the volume of melt, facilitating continued chemical communication and thus equilibrium [44]. However, the extraction traps in our experiments were included to serve as a suction pump to assure sufficient reaction of the lamproite melt during complete passage through the peridotite section, rather than to assess equilibrium melt compositions. Nevertheless, the melt compositions in the melt traps may approach equilibrium, as the volume of the pore space is estimated to be only 1–1.5% of the original volume of lamproite melt in the whole experiment. The melt compositions in the melt traps are modified from the original lamproite by reaction with the peridotite and may include components of the peridotite that were dissolved, rather than melted out, at temperatures below the peridotite solidus.

4.2. Melt Compositions before and after Reaction with Peridotite

The time-series experiments G138 (24 h), G131 (58 h) and G137 (132 h) had similar proportions of lamproite, peridotite and carbon traps in the starting materials and the melt compositions in the traps are broadly similar but show some significant inhomogeneities between melt pools. Baker and Stolper [20] noted that the SiO₂ content of melt in the extraction trap decreased in experiments with long durations, whereas the Al₂O₃ content increased. This could be the result of initial high-SiO₂ melt entering the trap first, followed by equilibration with a later melt from the rest of the run charge. This may indicate that the equilibrium concentrations of mobile elements such as alkalis or Ti should lie at the high end of the compositional variations displayed by the individual melt trap analyses (Figure 6). Ti, Na, K and Ba contents in melts in the melt trap increase with experimental duration, probably due to more extensive reaction during migration through the peridotite. In the shortest run of the time series, Opx has higher Al₂O₃ and Cr₂O₃ and lower FeO contents close to the carbon trap, which may be caused by the reaction with the percolating melt not having progressed as far as in the longer duration experiments.

The main differences in melt compositions at either side of the peridotite section are that the melt in the melt traps, which is modified by reaction with peridotite, has higher Mg#, Al₂O₃, Cr₂O₃ and Na₂O but lower K₂O and BaO. These reacted melts have less variable compositions than residual melts in the former lamproite section: this may be a function of quench modification in the larger areas of the latter, whereas melts quench well to glass in the melt trap. The higher and consistent Mg# is a result of buffering by the peridotite minerals, which are volumetrically dominant in the experiments. Peridotite minerals with Mg# ≈ 90 seek to impose an equilibrium Mg# of 70–73 on coexisting melts: the Mg# of the lamproite flowing in is slightly lower than this and is reduced further by the formation of high-Mg# phlogopite. The peridotite, therefore, removes Fe from the melt, forming the thin Fe-rich rims seen in BSE images (Figure 2) and the resultant melt in the melt trap has a higher and consistent Mg# (Figure 6b). If the melt/rock ratio were lower (corresponding to lower temperatures close to the lamproite solidus), this process would induce freezing of the melt and thus stoppage of the metasomatic process [44]. The lower contents of K₂O and BaO in the melt are due to the formation of metasomatic phlogopite, whereas the increase in Al₂O₃ and Cr₂O₃ is caused by the removal of garnet through reaction with the melt.

No phosphorus-bearing mineral was found in the experiments, but the concentration of ca. 0.6 wt% in melts in the extraction traps indicates dilution by a factor of two compared to the original leucite lamproite. This degree of dilution of phosphorus may mean that the contribution of peridotite to the melt is relatively high.

4.3. Applications to Mantle Metasomatism

4.3.1. Composition of Phlogopites Formed by Melt/Rock Reaction

The main aim of this study was to assess whether the phlogopites in cratonic garnet peridotites were formed by reaction with a passing potassic silicate melt. The phlogopites in

the lamproite section reflect magmatic crystallization from the lamproite melt, whereas the phlogopites occurring interstitially in the peridotite are the product of a reaction between melt and peridotite as the melt moves through the garnet peridotite and into the extraction trap. This is formed by the reaction of lamproitic melt primarily with garnet: the garnet reacts with the alkali- and water-rich melt and the high Cr_2O_3 content of the garnet (Table 2) is incorporated into the newly formed phlogopite. This conclusion is backed up by the observation that the interstitial phlogopite is xenomorphic (Figure 2) and has a much higher Cr_2O_3 content than the original lamproite (0.03 wt%; Table 2). At 2 GPa, the reaction also consumes Opx, whereas at 3 GPa Opx survives, indicating increased stability of Opx towards higher pressures, as is typical in peridotites [45].

Phlogopites in cratonic peridotites have been studied for several decades. Carswell [46] defined primary-textured micas as being single large crystals that have regular boundaries with silicate and oxide minerals, whereas secondary-textured micas usually form reaction rims around other silicate minerals, particularly orthopyroxene and garnet, and often occur as veinlets in the peridotite. Delaney et al. [4] showed that the compositions of these phlogopites show lower TiO_2 and higher Cr_2O_3 contents in later minerals, as judged by textures, and interpreted the high Cr_2O_3 micas to be the products of metasomatism by K- and H_2O -rich fluids in which the garnet reacts with the fluid (or melt). Later studies of other localities confirmed the higher Cr_2O_3 contents but found that the behaviour of TiO_2 was inconsistent, often also increasing in late micas (Figure 8; [47–50]). Micas in kelyphitic rims around garnets have particularly high Cr_2O_3 , extending up to 3 wt% in examples from ilmenite-rutile-phlogopite-sulphide series xenoliths despite lower concentrations of <0.75 wt% in primary-textured micas [51].

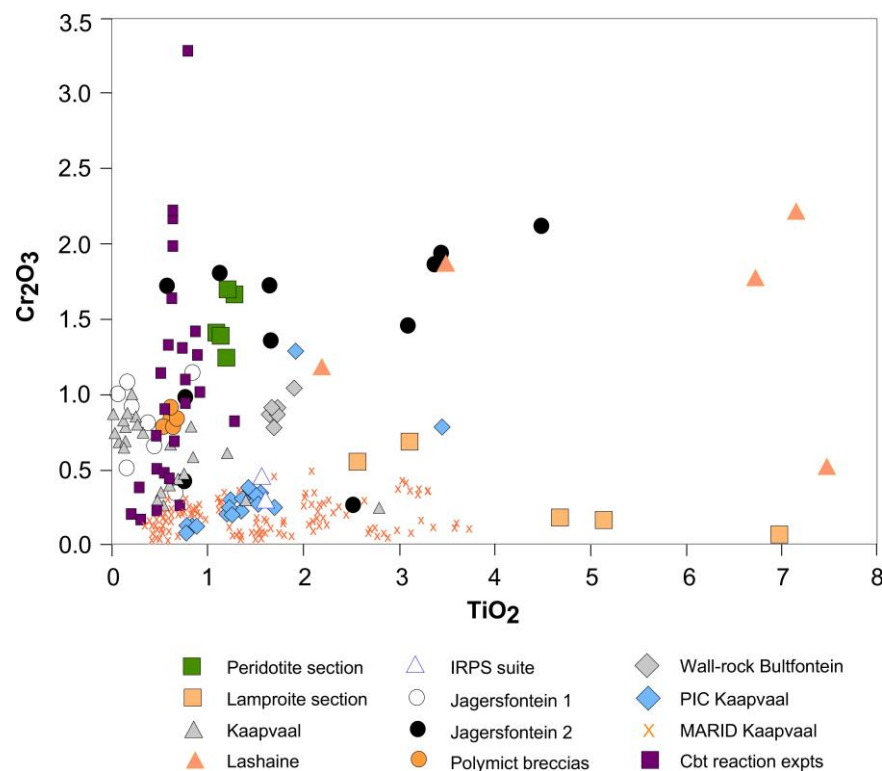


Figure 8. Comparison of phlogopites in peridotite (green squares) and lamproite (yellow squares) sections of the current experiments with phlogopites in natural mantle rocks. Data sources: Metasomatised Kaapvaal peridotites [4,50]; Lashaine peridotites [47]; Jagersfontein peridotites (1 = primary, 2 = secondary; [50]); IRPS suite [51]; Bultfontein peridotite close to vein, and polymict breccias [48]; MARID and PIC xenoliths [52]; experiments reacting carbonate-silicate melt with peridotite (“cbt reaction expts”; [53]).

Erlank et al. [5] describe the metasomatic progression from garnet peridotites (GP), through garnet phlogopite peridotites (GPP) and phlogopite peridotites (PP) to phlogopite K-richterite peridotites (PKP), resulting from increasing metasomatic alteration by alkali-, volatile- and incompatible element-rich fluids, which were re-interpreted as melts by [6]. The experimental results presented here are the equivalent of phlogopite peridotite, where metasomatic alteration has removed the garnet completely.

The phlogopites occurring interstitially in the current experiments have similar trends of decreasing TiO₂ and increasing Cr₂O₃ relative to phlogopites in the lamproite section and plot towards the upper end of Cr₂O₃ contents of secondary-textured micas in the natural peridotites (Figure 8). They may be equivalent to those in kelyphitic rims, but garnet was completely replaced by phlogopites under these experimental conditions, as a result of the relatively high temperature and low pressure [54]. Rapid breakdown of garnet is facilitated by the presence of the melt, which has been shown to react 100 µm in 2 days at 1050 °C [55], a distance exceeding the grain size of the garnets in our starting materials.

4.3.2. Reactivity of Different Alkaline Melts with Peridotite

There are a range of melts that may be involved in the metasomatic process when they infiltrate peridotites, and these melts should produce different mineralogical assemblages. Current summaries of metasomatic types in peridotites of the Kaapvaal Craton in South Africa recognize principally two types of phlogopite-bearing assemblages, known as MARID (mica-amphibole-rutile-ilmenite-diopside) and PIC (phlogopite-ilmenite-clinoproxene) [9,53], although other minor types (e.g., IRPS; [51]) may have been neglected. Candidates for melt types for cratonic processes include kimberlite, orangeite (formerly Group II kimberlite), lamproite, as well as carbonate-rich melts such as carbonatites and carbonated silicate melts with <30 wt% SiO₂ that are recognized as potential metasomatic agents from high-pressure experiments more than from natural rocks [56,57].

The formation of PIC and MARID xenolith suites has been assigned to interaction with kimberlites and orangeite melts, respectively [9]. However, orangeites and lamproites may be related, although the exact relationship is currently uncertain. Some refer to them as carbonate-rich lamproites [13,58], a Kaapvaal equivalent of carbonate-poor lamproites elsewhere that have been shown to originate in reduced source regions where carbonate would not be stable [24,59]. This mode of origin also occurs in eastern Zambia [60].

Few studies that produced phlogopites from the reaction between melts and peridotite are available for comparison with our experimental results. Odling [16] reacted kimberlite melts (25 wt% SiO₂, 5.9 wt% CO₂, 6.5 wt% H₂O) with harzburgite in experiments with a temperature gradient, finding interstitial phlogopite and glass coexisting with olivine+Cpx+Sp at high temperatures, which transitioned to Ol+Cpx+Phl and were joined by orthopyroxene and finally K-richterite at a lower temperature. Shatskiy et al. [53] studied the interaction of a synthetic potassic carbonatite (0% SiO₂, 35–44 wt% CO₂, 8.1–11.6 wt% H₂O, 0–4.9 wt% Na₂O) mixed at different proportions with peridotite, finding K-richterite in addition to phlogopite and carbonates, but only if Na₂O-bearing carbonatite melts were used. Other experiments using dry carbonatite or carbonated silicate melts and peridotite did not produce phlogopite [37].

Shatskiy et al. [53] confirmed the observation that Cr₂O₃ in phlogopite is highest where garnet was consumed, implying a similar interpretation for the natural phlogopites of [4] but involving a carbonatite melt in contrast to our CO₂-free lamproite melt. K-richterite was found as a product of reaction with kimberlite [16] and carbonatite [53] but not in our experiments with lamproitic melt, which is noteworthy since K-richterite occurs in lamproites but not in kimberlites or carbonatites. The phlogopites in all three studies of reaction experiments are enriched in Cr₂O₃ (Figure 8; Odling's single analysis had 1.51 wt%), whereas there is a small but distinct difference in TiO₂. Those in the current experiments have 1.07–1.26 wt % TiO₂, presumably due to the high TiO₂ in the lamproite, whereas those resulting from reaction with carbonatite have an average of 0.61 wt% and with kimberlite 0.21 wt%. This difference, together

with any inclusions of Cr-spinel or especially carbonates, as in the experiments of [53], may prove critical in deciding which melt type drove the metasomatic reactions in natural rocks.

4.3.3. Compositional Evolution of the Reacting Melt

A principal difference between the current experimental design and other experiments on metasomatic reactions is the inclusion of the carbon melt trap at the far end of the capsules in which melt compositions were analyzed. Although intended primarily to assist the flow of the melt through the peridotite, this melt trap collected the evolved melt. Initial melts entering the trap may have been artificially high in SiO₂, corresponding to a lower effective pressure because of the initial pore space in the trap [19]. After it was filled, the time series experiments show that the melt composition changed to approach the correct composition, with Ti, Na, K and Ba needing longer to reach equilibrium because of exchange reactions with the peridotite. Melts in the trap were inhomogeneous, varying between different pools that had experienced different paths through the peridotite (Figure 5).

The compositions of melts in the trap show increased Mg# and lower BaO contents, K₂O/Na₂O and K/Al ratios relative to the initial lamproite melt composition (Figure 6) because of the loss of chemical components to phlogopite during melt/rock reaction. The Mg# would remain buffered at high values as long as melt percolates along grain boundaries rather than flowing through coated channels.

The experiments could also be seen to represent an advanced stage of melting of phlogopite and K-richterite-bearing hydrous pyroxenite vein [18], from which the melt infiltrates the peridotite wall-rock and partially dissolves it [61]. At this advanced state of melting when phlogopite remains the only stable phase in the vein assemblage, the experiments confirm predictions [44] that the melt will dissolve mainly garnet and orthopyroxene. The melt in the carbon trap would then represent melt that moves on to higher levels of the lithosphere in the case of percolation along grain boundaries. This shows that the vein/wall-rock reaction is not a matter of simple dissolution of minerals, because phlogopite forms during the reaction, involving the dissolution of olivine. This would deplete the melt in K₂O and BaO, which does not correspond to the extreme enrichment in K₂O and BaO in lamproites [17]. However, this may be explained by the movement of melt through coated channels initially produced by high melt flow rates: lamproitic melt compositions are consistent with the melting of K-richterite-bearing rocks, which produce a large melt fraction with little rise in temperature above the solidus [18]. Following initial infiltration and reaction with wall rocks, melts with high K₂O/Na₂O will be channeled in the little-modified form to higher levels. The current experiments indicate that at lower rates of melt infiltration, alkaline melts with lower K₂O/Na₂O may evolve through melt/rock reactions.

5. Conclusions

Flow-through experiments reproducing the reaction of migrating lamproitic melt and peridotite wall rocks were conducted with a vitreous carbon melt trap at the opposite end of the experimental capsule to the lamproitic melt to assist the migration of the melt. This set-up also allowed chemical analysis of the melt after reaction with the peridotite, which showed increased Mg#, decreased K₂O/Na₂O and decreased K/Al ratios relative to the unreacted lamproite melt. The melts in the traps show that lamproitic melts lose the chemical characteristics of lamproites through this reaction, indicating that lamproites are unlikely to be derived from a peridotite source, but more likely a source dominated by phlogopite-rich hydrous pyroxenites.

Reactions in the peridotite removed orthopyroxene and garnet and deposited phlogopite by an incongruent reaction of melt with olivine and orthopyroxene. The phlogopites formed mimic the compositions of those seen in peridotite xenoliths, with increased Cr₂O₃ derived from the garnets.

Author Contributions: Conceptualisation, S.F.F.; formal analysis, S.F.F. and M.P.; investigation, M.P. and S.F.F.; data curation, S.F.F.; writing—original draft preparation, S.F.F. and M.P.; writing—review

and editing, S.F.F.; project administration, S.F.F.; funding acquisition, S.F.F. All authors have read and agreed to the published version of the manuscript.

Funding: This research was funded by the Deutsche Forschungsgemeinschaft Grant Fo 181-3 and Australian Research Council Grant FL180100134 to S. Foley.

Institutional Review Board Statement: Not applicable.

Informed Consent Statement: Not applicable.

Data Availability Statement: Not applicable.

Acknowledgments: This paper is based on the Diploma (M.Sc.) thesis of M.P. [27]. John Sheraton and Gerhard Brey supplied the lamproite and peridotite samples used in the experiments. We thank Michael Förster, Chunfei Chen and Isra Ezad for their comments on the manuscript.

Conflicts of Interest: The authors declare no conflict of interest.

References

- O'Reilly, S.Y.; Griffin, W.L. Mantle metasomatism. In *Metasomatism and the Chemical Transformation of Rock*; Harlov, D.E., Austrheim, H., Eds.; Springer: Heidelberg, Germany, 2013; pp. 471–533.
- Simon, N.S.C.; Carlson, R.W.; Pearson, D.G.; Davies, G.R. The origin and evolution of the Kaapvaal cratonic lithospheric mantle. *J. Petrol.* **2007**, *48*, 589–625. [[CrossRef](#)]
- Rehfeldt, T.; Foley, S.F.; Carlson, R.W.; Lowry, D.; Jacob, D.E. Contrasting types of metasomatism in dunite, wehrlite and websterite xenoliths from Kimberley, South Africa. *Geochim. Cosmochim. Acta* **2008**, *72*, 5722–5756. [[CrossRef](#)]
- Delaney, J.S.; Smith, J.V.; Carswell, D.A.; Dawson, J.B. Chemistry of micas from kimberlites and xenoliths—II. Primary- and secondary-textured micas from peridotite xenoliths. *Geochim. Cosmochim. Acta* **1980**, *44*, 857–872. [[CrossRef](#)]
- Erlank, A.J.; Waters, F.G.; Hawkesworth, C.J.; Haggerty, S.E.; Allsopp, H.; Rickard, R.S.; Menzies, M.A. Evidence for mantle metasomatism in peridotite nodules from the Kimberley pipes, South Africa. In *Mantle Metasomatism*; Menzies, M.A., Hawkesworth, C.J., Eds.; Academic Press: London, UK, 1987; pp. 221–311.
- Waters, F.G.; Erlank, A.J.; Daniels, L.R.M. Contact relationships between MARID rock and metasomatised peridotite in a kimberlite xenolith. *Geochem. J.* **1989**, *23*, 11–17. [[CrossRef](#)]
- Harte, B.; Hunter, R.H.; Kinny, P.D. Melt geometry, movement and crystallization, in relation to mantle dykes, veins and metasomatism. *Phil. Trans. Roy. Soc. Lond. Ser. A* **1993**, *342*, 1–21.
- Harte, B. Mantle peridotites and processes—the kimberlite sample. In *Continental Basalts and Mantle Xenoliths*; Hawkesworth, C.J., Norry, M.J., Eds.; Shiva: Nantwich, UK, 1983; pp. 46–91.
- Gregoire, M.; Bell, D.R.; Le Roex, A.P. Trace element geochemistry of phlogopite-rich mafic mantle xenoliths: Their classification and their relationship to phlogopite-bearing peridotites and kimberlites revisited. *Contrib. Mineral. Petrol.* **2002**, *142*, 603–625. [[CrossRef](#)]
- Waters, F.G. A suggested origin of MARID xenoliths in kimberlites by high pressure crystallization of an ultrapotassic rock such as lamproite. *Contrib. Mineral. Petrol.* **1987**, *95*, 523–533. [[CrossRef](#)]
- Giuliani, A.; Phillips, D.; Woodhead, J.D.; Kamenetsky, V.S.; Fiorentini, M.L.; Maas, R.; Soltys, A.; Armstrong, R.A. Did diamond-bearing orangeites originate from MARID-veined peridotites in the lithospheric mantle? *Nature Comm.* **2015**, *6*, 6837. [[CrossRef](#)]
- Mitchell, R.H. *Kimberlites, Orangeites and Related Rocks*; Plenum Press: New York, NY, USA; London, UK, 1995; p. 410.
- Pearson, D.G.; Woodhead, J.; Janney, P.E. Kimberlites as geochemical probes of Earth's mantle. *Elements* **2019**, *15*, 387–392. [[CrossRef](#)]
- Borghini, G.; Rampone, E.; Zanetti, A.; Class, C.; Fumagalli, P.; Godard, M. Ligurian pyroxenite-peridotite sequences (Italt) and the role of melt-rock reaction in creating enriched-MORB mantle sources. *Chem. Geol.* **2020**, *532*, 119252. [[CrossRef](#)]
- Odling, N.W.A. An experimental simulation of upper mantle metasomatism. *Amer. Mineral.* **1994**, *79*, 148–153.
- Odling, N.W.A. An experimental replication of upper mantle metasomatism. *Nature* **1995**, *373*, 58–60. [[CrossRef](#)]
- Jaques, A.L.; Lewis, J.D.; Smith, C.B. The kimberlites and lamproites of Western Australia. *Geol. Surv. Western Aus. Bull.* **1986**, *132*, 268.
- Foley, S.F.; Ezad, I.S.; van der Laan, S.R.; Pertermann, M. Melting of hydrous pyroxenite assemblages with alkali amphiboles in the continental mantle lithosphere. Part 1: Melting relations and major element compositions of melts. Unpublished work. 2021.
- Falloon, T.J.; Green, D.H.; Danyushevsky, L.V.; Faul, U.H. Peridotite melting at 1.0 and 1.5 GPa: An experimental evaluation of techniques using diamond aggregates and mineral mixes for determination of near-solidus melts. *J. Petrol.* **1999**, *40*, 1343–1375. [[CrossRef](#)]
- Baker, M.B.; Stolper, E.M. Determining the composition of high-pressure mantle melts using diamond aggregates. *Geochim Cosmochim Acta* **1994**, *58*, 2811–2827. [[CrossRef](#)]
- Hirose, K.; Kushiro, I. Partial melting of dry peridotites at high pressures: Determination of compositions of melts segregated from peridotite using aggregates of diamond. *Earth Planet. Sci. Lett.* **1997**, *114*, 477–489. [[CrossRef](#)]

22. Van den Bleeken, G.; Müntener, O.; Ulmer, P. Reaction processes between tholeiitic melt and residual peridotite in the uppermost mantle: An experimental study at 0.8 GPa. *J. Petrol.* **2010**, *51*, 153–183. [[CrossRef](#)]
23. Van den Bleeken, G.; Müntener, O.; Ulmer, P. Melt variability in percolated peridotite: An experimental study applied to reactive migration of tholeiitic basalt in the upper mantle. *Contrib. Mineral. Petrol.* **2011**, *161*, 921–945. [[CrossRef](#)]
24. Foley, S.F. The genesis of lamproitic magmas in a reduced, fluorine-rich mantle. In *Kimberlites and Related Rocks*; Ross, J., Ed.; Blackwell: Melbourne, Australia, 1989; Volume 1, pp. 616–632.
25. Mallik, A.; Dasgupta, R. Effect of variable CO₂ on eclogite-derived andesite and lherzolite reaction at 3 GPa—implications for mantle source characteristics of alkali ocean island basalts. *Geochem. Geophys. Geosys.* **2014**, *15*, 1533–1557. [[CrossRef](#)]
26. Wang, Y.; Prelevic, D.; Buhre, S.; Foley, S.F. Constraints on the sources of post-collisional K-rich magmatism: The roles of continental clastic sediments and terrigenous blueschists. *Chem. Geol.* **2017**, *455*, 192–207. [[CrossRef](#)]
27. Pertermann, M. High-Pressure Experiments on the Origin of Metasomatic Melts in the Mantle. An Experimental Investigation in Two Parts. Diploma Thesis, Mineralogisch-Petrologisches Institute, Universität Göttingen, Göttingen, Germany, 1997; p. 76.
28. Foley, S. An experimental study of olivine lamproite—first results from the diamond stability field. *Geochim. Cosmochim. Acta* **1993**, *57*, 483–489. [[CrossRef](#)]
29. Sheraton, J.W.; Cundari, A. Leucitites from Gaussberg, Antarctica. *Contrib. Mineral. Petrol.* **1980**, *71*, 417–427. [[CrossRef](#)]
30. Wang, Y.; Foley, S.F. Hybridization melting between continent-derived sediment and depleted peridotite in subduction zones. *J. Geophys. Res.* **2018**, *123*, 3414–3429. [[CrossRef](#)]
31. Sekine, T.; Wyllie, P.J. Experimental simulation of mantle hybridization in subduction zones. *J. Geol.* **1983**, *91*, 511–528. [[CrossRef](#)]
32. Bulatov, V.K.; Brey, G.P.; Girmis, A.V.; Gerdes, A.; Höfer, H. Carbonated sediment-peridotite interaction and melting at 7.5–12 GPa. *Lithos* **2014**, *200–201*, 368–385. [[CrossRef](#)]
33. Castro, A.; Gerya, T.V. Magmatic implications of mantle wedge plumes: Experimental study. *Lithos* **2008**, *103*, 138–148. [[CrossRef](#)]
34. Förster, M.W.; Prelevic, D.; Schmück, H.R.; Buhre, S.; Veter, M.; Mertz-Kraus, R.; Foley, S.F.; Jacob, D.E. Melting and dynamic metasomatism of mixed harzburgite+glimmerite mantle source: Implications for the origin of orogenic potassic magmas. *Chem. Geol.* **2017**, *455*, 182–191. [[CrossRef](#)]
35. Förster, M.W.; Prelevic, D.; Buhre, S.; Mertz-Kraus, R.; Foley, S.F. An experimental study of the role of partial melts of sediments versus mantle melts as sources of potassic magmatism. *J. Asian Earth Sci.* **2019**, *177*, 76–88. [[CrossRef](#)]
36. Förster, M.W.; Bussweiler, Y.; Prelevic, D.; Daczko, N.R.; Buhre, S.; Mertz-Kraus, R.; Foley, S.F. Sediment-peridotite reaction controls fore-arc metasomatism and arc-magma geochemical signatures. *Geosciences* **2021**, in press.
37. Gervasoni, F.; Klemme, S.; Rohrbach, A.; Grützner, T.; Berndt, J. Experimental constraints on mantle metasomatism caused by silicate and carbonate melts. *Lithos* **2017**, *282–283*, 173–186. [[CrossRef](#)]
38. Johnston, A.D.; Wyllie, P.J. The system tonalite-peridotite-H₂O at 30 kbar, with applications to hybridization in subduction zone magmatism. *Contrib. Mineral. Petrol.* **1989**, *102*, 257–264. [[CrossRef](#)]
39. Mallik, A.; Dasgupta, R. Reaction between MORB-eclogite derived melts and fertile peridotite and generation of ocean island basalts. *Earth Planet. Sci. Lett.* **2012**, *329–330*, 97–108. [[CrossRef](#)]
40. Mallik, A.; Dasgupta, R. Reactive infiltration of MORB-eclogite-derived carbonated silicate melt into fertile peridotite at 3GPa and genesis of alkali magmas. *J. Petrol.* **2013**, *54*, 2267–2300. [[CrossRef](#)]
41. Gao, M.D.; Xu, H.; Zhang, J.F.; Foley, S.F. Experimental interaction of granitic melt and peridotite at 1.5 GPa: Implications for the origin of post-collisional K-rich magmatism in continental subduction zones. *Lithos* **2019**, *350–351*, 105241. [[CrossRef](#)]
42. Ryabchikov, I.D.; Orlova, G.P.; Kalenchuk, G.Y.; Ganeyev, I.I.; Udovkina, N.G.; Nosik, L.P. Reactions of spinel lherzolite with H₂O-CO₂ fluids at 20 kbar and 900 °C. *Geochem. Internat.* **1989**, 56–62.
43. Kushiro, I.; Hirose, K. Experimental determination of composition of melt formed by equilibrium partial melting of peridotite at high pressures using aggregates of diamond grains. *Proc. Japan Acad. Ser. B* **1992**, *68*, 63–68. [[CrossRef](#)]
44. Foley, S.F.; Musselwhite, D.S.; van der Laan, S.R. Melt compositions from ultramafic vein assemblages in the lithospheric mantle: A comparison of cratonic and non-cratonic settings. In *J.B. Dawson Volume, Proceedings of the Cape Town Kimberlite Conference*; Red Roof Publishers: Cape Town, South Africa, 1999; pp. 238–246.
45. Walter, M.J. Melt extraction and compositional variability in mantle lithosphere. *Treatise Geochem.* **2003**, *2*, 363–394.
46. Carswell, D.A. Primary and secondary phlogopites and clinopyroxenes in garnet lherzolite xenoliths. *Phys. Chem. Earth* **1975**, *9*, 417–430. [[CrossRef](#)]
47. Dawson, J.B. Metasomatism and partial melting in upper-mantle peridotite xenoliths from the Lshaine volcano, northern Tanzania. *J. Petrol.* **2002**, *43*, 1749–1777. [[CrossRef](#)]
48. Giuliani, A.; Phillips, D.; Kamenetsky, V.S.; Kendrick, M.A.; Wyatt, B.A.; Goemann, K.; Hutchinson, G. Petrogenesis of mantle polymict breccias: Insights into mantle processes coeval with kimberlite magmatism. *J. Petrol.* **2014**, *55*, 831–858. [[CrossRef](#)]
49. Field, S.W.; Haggerty, S.E.; Erlank, A.J. Subcontinental metasomatism in the region of Jagersfontein, South Africa. In *Kimberlites and Related Rocks 2*; Ross, J., Ed.; Blackwell: Melbourne, Australia, 1989; pp. 771–783.
50. Jones, A.P.; Smith, J.V.; Dawson, J.B. Mantle metasomatism in 14 veined peridotites from Bultfontein Mine, South Africa. *J. Geol.* **1982**, *90*, 435–453. [[CrossRef](#)]
51. Harte, B.; Winterburn, P.A.; Gurney, J.J. Metasomatic and enrichment phenomena in garnet peridotite facies mantle xenoliths from the Matsoku kimberlite pipe Lesotho. In *Mantle Metasomatism*; Menzies, M.A., Hawkesworth, C.J., Eds.; Academic Press: London, UK, 1987; pp. 145–220.

52. Fitzpayne, A.; Giuliani, A.; Hergt, J.; Phillips, D.; Janney, P. New geochemical constraints on the origins of MARID and PIC rocks: Implications for mantle metasomatism and mantle-derived potassic magmatism. *Lithos* **2018**, *318–319*, 478–493. [[CrossRef](#)]
53. Shatskiy, A.; Bekhtenova, A.; Arefiev, A.V.; Podborodnikov, I.V.; Vinogradova, Y.G.; Rezvukhin, D.I.; Litasov, K.D. Solidus and melting of carbonated phlogopite peridotite at 3–6.5 GPa: Implications for mantle metasomatism. *Gondwana Res.* **2022**, *101*, 156–174. [[CrossRef](#)]
54. Zibera, L.; Klemme, S.; Nimis, P. Garnet and sinel in fertile and depleted mantle: Insights from thermodynamic modelling. *Contrib. Mineral. Petrol.* **2013**, *166*, 411–421. [[CrossRef](#)]
55. Ezad, I.S.; Dobson, D.P.; Thompson, A.R.; Jennings, E.S.; Hunt, S.A.; Brodholt, J.P. Kelyphite textures experimentally reproduced through garnet breakdown in the presence of a transient melt phase. *J. Petrol.* **2021**, in press.
56. Dasgupta, R.; Hirschmann, M.M. Effect of variable carbonate concentration on the solidus of mantle peridotite. *Amer. Mineral.* **2007**, *92*, 370–379. [[CrossRef](#)]
57. Pintér, Z.; Foley, S.F.; Yaxley, G.M.; Rosenthal, A.; Rapp, R.P.; Lanati, A.W.; Rushmer, T. Experimental investigation of the composition of incipient melts in upper mantle peridotites in the presence of CO₂ and H₂O. *Lithos* **2021**, *396–397*, 106224. [[CrossRef](#)]
58. Mitchell, R.H. Igneous rock associations 26. Lamproites, exotic potassic alkaline rocks: A review of their nomenclature, characterization and origins. *Geosci. Can.* **2020**, *47*, 119–142. [[CrossRef](#)]
59. Foley, S.F. Experimental constraints on phlogopite chemistry in lamproites: 1. The effect of water activity and oxygen fugacity. *Eur. J. Mineral.* **1989**, *1*, 411–426. [[CrossRef](#)]
60. Ngwenya, N.S.; Tappe, S. Diamondiferous lamproites of the Luangwa Rift in central Africa and links to remobilized cratonic lithosphere. *Chem. Geol.* **2021**, *568*, 120019. [[CrossRef](#)]
61. Foley, S. Vein-plus-wall-rock melting mechanisms in the lithosphere and the origin of potassic alkaline magmas. *Lithos* **1992**, *28*, 435–453. [[CrossRef](#)]